Supplement of Atmos. Chem. Phys., 19, 315–325, 2019
https://doi.org/10.5194/acp-19-315-2019-supplement

Atmospheric Chemistry and Physics
Open Access

Supplement of

Diel variation in mercury stable isotope ratios records photoreduction of $PM_{2.5}$-bound mercury

Qiang Huang et al.

Correspondence to: Jiubin Chen (jbchen@tju.edu.cn)

1. Materials and methods

1.1 Materials

HCl, HNO_3 and stannous chloride ($SnCl_2$) were analytical grade (Sinopharm Chemical Reagent Co., Ltd., China). Milli-Q water (18.2 MΩ, Millipore, USA) was used for preparation all aqueous solutions. Concentrated HCl and HNO_3 were double-distilled using a DST-1000 acid purification system (Savillex, USA). Two $SnCl_2$ solutions of 0.20 and 0.03 g/mL were prepared by dissolving the solid $SnCl_2$ in 1 M HCl and were used for online reduction of Hg^{2+} during the content and isotope measurements, respectively. The National Institute of Standards and Technology Standard Reference Material 3133 (NIST SRM 3133) Hg and UM-Almaden Hg were used as international standards and measured regularly to control the accuracy and quality of isotope analysis. Two other reference materials, the solution NIST SRM 3177 Hg and the Yellow-Red Soil GBW07405 (National Center for Standard Materials, Beijing, China) were used as in-house isotope standards, and were regularly measured for quality control of Hg content and isotope measurements. GBW07405 was also used as procedure standard to evaluate the accuracy and precision of sample pretreatment (Huang et al., 2015; Huang et al., 2016). The NIST SRM 997 Thallium (20 ng mL^{-1} Tl in 3 % HNO_3) was employed as an internal standard for mass bias correction.

1.2 Sample pretreatment for mercury isotopes analysis

After collection, mercury bound on $PM_{2.5}$ with sufficient mass for isotopic analysis (≥ 10 ng) was concentrated into a 5-mL 40% acid mixture (2:4:9 volumetric ratio of 10 M HCl, 15 M HNO_3 and Milli-Q water) according to the methods reported in Huang et al. (2015). Schematic diagram of the combustion-trapping assembly from Huang et al. (2015) is shown below. To extract Hg bound to PM samples, each filter was rolled into a cylinder and placed in a sample quartz tube. Both ends of the tube were capped with quartz wool (pre-cleaned at 500°C) to prevent particle emission. Each tube was combusted over 2 h in a temperature-programmed dual-stage quartz tube combustion furnace in which the temperature of the first furnace was incrementally increased to 900°C whereas the second furnace was held at 950°C. The resulting Hg vapor was swept by O_2 gas (Hg free) into the 40% acid trapping solution. The trapping solution was diluted with Milli-Q H_2O to 10 mL to a final acid concentration of 20%. The accuracy and precision of the dual-stage combustion protocol were evaluated by the analysis of the GBW07405 using the same digestion method. The detection limit given by the procedural blanks (< 0.3 ng) for this dual-stage combustion method was negligibly low compared to the total Hg mass (≥ 10 ng) extracted from either $PM_{2.5}$ samples or procedural standards.

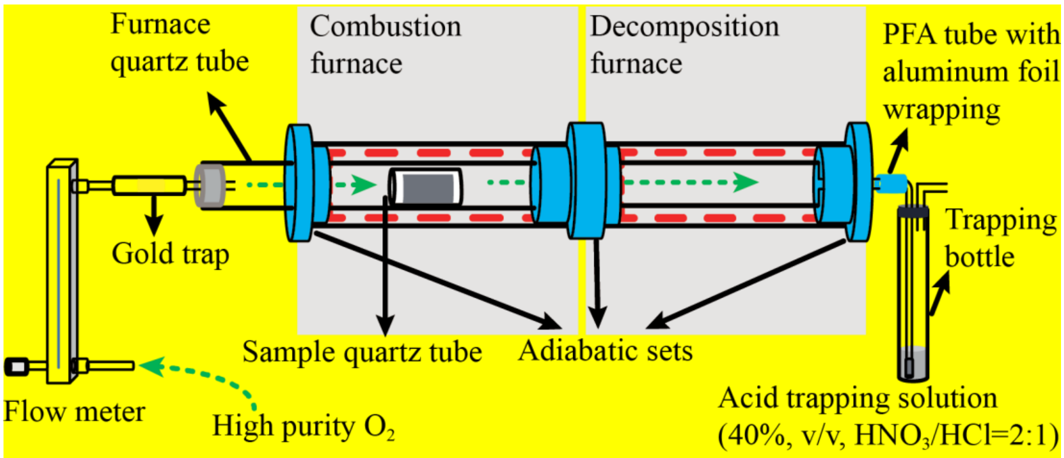

Schematic diagram of the combustion-trapping assembly from Huang et al. (2015).

1.3 Mercury concentration and stable isotope composition measurements

The methods used to measure the Hg content and isotope ratio were published elsewhere (Huang et al., 2015). In brief, a small fraction of each trapping solution (20% acid mixture) was used to measure the Hg content on cold-vapor atomic fluorescence spectroscopy (CVAFS, Tekran 2500, Tekran® Instruments Corporation, CA), with a precision better than 10%. The recoveries of Hg for the standard GBW07405 were in the acceptable range of 95 to 105% with an average value of 98% (1 SD = 6%, n = 6); but no recovery of Hg for the $PM_{2.5}$ samples was determined due to limited availability of the samples.

A total of 61 $PM_{2.5}$ samples were collected during the sampling campaign. After analysis of Hg contents, we found that 56 $PM_{2.5}$ samples (including 26 daytime and 30 nighttime samples) have sufficient Hg mass and hence were further analyzed for Hg isotope compositions using a multicollector inductively coupled plasma mass spectrometer (MC-ICP-MS, Nu Instruments Ltd., UK) equipped with a continuous flow cold vapor generation system. Detailed protocols for the Hg isotope analysis can be found in Huang et al. (2015). The Faraday cups were positioned to simultaneously collect five Hg isotopes and two Tl isotopes including ^{205}Tl (H3), ^{203}Tl (H1), ^{202}Hg (Ax), ^{201}Hg (L1), ^{200}Hg (L2), ^{199}Hg (L3), and ^{198}Hg (L4). ^{196}Hg and ^{204}Hg were not measured due to their very low abundance. Instrumental mass bias was corrected using an internal standard (NIST SRM 997 Tl) and strict sample-standard bracketing with NIST SRM 3133 Hg standard. For quality assurance and control, the well-known reference material UM-Almaden and the NIST SRM 3177 Hg were inserted repeatedly into the sampling list after every ten and five real samples, measured regularly during sample analysis session, and calibrated periodically against the NIST SRM 3133 Hg as well as samples.

Delta (δ) notation is used to represent MDF in units of per mil (‰) as defined by the following equation (Blum and Bergquist, 2007):

$$\delta^{x}\text{Hg (‰)} = [(^{x}\text{Hg}/^{198}\text{Hg})_{\text{sample}}/(^{x}\text{Hg}/^{198}\text{Hg})_{\text{NIST3133}} - 1] \times 1000 \qquad (1)$$

where x = 199, 200, 201, and 202. MIF is reported as the deviation of a measured delta value from the theoretically predicted MDF value according to the equation:

$$\Delta^{x}Hg\ (‰) = \delta^{x}Hg - \beta \times \delta^{202}Hg \quad (2)$$

where the mass-dependent scaling factor β is 0.252, 0.5024, and 0.752 for ^{199}Hg, ^{200}Hg and ^{201}Hg, respectively (Blum and Bergquist, 2007).

1.4 Backward trajectory analysis

The backward HYSPLIT trajectories of air masses at a height of 500 m above ground level and arriving at the sampling site (at 39.9725 N 116.3683 E) were simulated. Because the average boundary layer heights was reported about 500 m in Beijing (Xiang et al., 2019), so the arrival height of 500 m used for backward HYSPLIT trajectories of air masses could be acceptable in this study. In fact, different arrival heights (200, 500, 1000 m AGL) of backward trajectories were tested and results indicated that the transport pathways were not very sensitive to the selected heights within the studied area. Backward trajectories for each sample, ending at 1100 UTC (equal to local time 7:00 p.m.) for daytime sample and ending at 2300 UTC (equal to local time 7:00 a.m.) for nighttime sample, were calculated every 1 hrs using the Internet-Based HYSPLIT Trajectory Model and gridded meteorological data (Global Data Assimilation System, GDAS1) from the U.S. National Oceanic and Atmospheric Administration (NOAA) and were shown below (Fig. S1). The obtained average directions of arriving air masses for each sample were summarized in Table S1. The frequencies of backward trajectories were also calculated for all the samples taken during Sept. 15th to Oct. 16th 2015 using the Internet-Based HYSPLIT Trajectory Model and the archived GDAS0p5, with an interval of 3 hrs, each trajectory total run time 72 hrs and a 0.5 × 0.5 degree trajectory frequency grid resolution. The results of such simulation showed the dominating air mass arriving from southwest of the sampling site (see Fig. 1).

1.5 GOM calculation

We used an inverse approach and a GOM partitioning model to compute hypothetic GOM levels corresponding to each of our PBM observations at ambient temperature. We used the GOM gas-aerosol partitioning model proposed by Amos et al. (2012), which has the following equation: $\log_{10}(K^{-1}) = (10\pm1) - (2500\pm300)/T$, where $K = (PBM/PM_{2.5})/GOM$ with PBM and GOM in common volumetric units (pg m^{-3}), $PM_{2.5}$ in μg m^{-3}, and T in K. We used the measured $PM_{2.5}$-Hg as PBM and assumed that the $PM_{2.5}$-Hg measured for each sample is 100% in divalent and active mercury forms. The calculated GOM concentrations are presented in the following Table S4. In summary, the calculated GOM concentrations range from 1.5 to 31 pg m^{-3}, with average values of 11±5 pg m^{-3} during the daytime and 13±7 pg m^{-3} during the nighttime. Overall, the calculated GOM exhibit insignificant (p = 0195, paired samples t-test) diel variation of GOM concentration, i.e., there would be little or no difference of GOM between day- and night-time. Close inspection of the data (Table S4) showed that half of the paired day-night samples have higher calculated GOM concentrations during the nighttime than in daytime.

Table S1. List of 61 $PM_{2.5}$ samples and their associated weather data.

Name	Sampling date	Start time	End time	Directions of arriving air mass	Weather	Sunshine duration (hrs)	SH (MJ/m^2)	O_3 (ppbv)	T (ºC)	RH (%)	MWS (m/s)	WS (m/s)
Sept-15-N	Sept-15-2015	19:02	7:02	S-SW	Cloudy			7.3	19.8	68	3.9	2
Sept-16-D	Sept-16-2015	8:25	18:55	SW	Sunny	8	6.40	67.7	24.1	52	3.9	2
Sept-16-N	Sept-16-2015	19:02	7:02	SW	Cloudy			5.6	21.1	70	3.9	2
Sept-17-D	Sept-17-2015	8:13	18:43	SW	Cloudy	4	3.02	72.3	24.8	56	4.0	2
Sept-17-N	Sept-17-2015	19:03	7:33	SW-NW	Cloudy+Rain			19.1	22.6	74	4.0	2
Sept-18-D	Sept-18-2015	8:19	18:49	N	Sunny	9	13.24	43.2	27.3	39	3.1	2
Sept-18-N	Sept-18-2015	18:57	7:27	N-NE	Clear			1.1	21.7	54	3.1	2
Sept-19-D	Sept-19-2015	8:07	18:37	NE-E	Sunny	11	17.20	41.5	26.1	33	3.6	1
Sept-19-N	Sept-19-2015	18:48	7:18	S	Clear			4.8	21.7	60	3.6	1
Sept-20-D	Sept-20-2015	8:04	18:34	SW	Cloudy	7	4.45	34.4	24.5	55	4.3	2
Sept-20-N	Sept-20-2015	18:42	7:12	SW	Cloudy			5.7	21.9	62	4.3	2
Sept-21-D	Sept-21-2015	8:17	18:47	SW	Sunny	9	6.04	41.3	25.2	49	4.1	2
Sept-21-N	Sept-21-2015	18:55	7:25	S	Cloudy			18.6	22.6	62	4.1	2
Sept-22-D	Sept-22-2015	8:18	18:18	S-SW	Overcast+Rain	0	0.43	31.4	22.9	70	5.4	2
Sept-22-N	Sept-22-2015	18:28	6:58	W-NW	Cloudy			6.3	18.3	86	5.4	2
Sept-23-D	Sept-23-2015	8:13	18:13	S-NW	Sunny	9	11.20	36.1	23.9	54	2.7	2
Sept-23-N	Sept-23-2015	18:13	6:56	S-SW	Cloudy			3.3	21.6	71	2.7	2
Sept-24-D	Sept-24-2015	8:07	18:07	S	Cloudy	2	0.73	26.5	23.0	72	3.8	2
Sept-24-N	Sept-24-2015	18:15	6:45	SE-W	Cloudy+Rain			19.4	17.7	87	3.8	2
Sept-25-D	Sept-25-2015	8:28	18:28	NW	Sunny	11	18.43	28.6	24.4	19	4.8	2
Sept-25-N	Sept-25-2015	19:03	7:33	SW-NW	Clear			1.2	17.3	44	4.8	2
Sept-26-D	Sept-26-2015	8:06	18:06	SW	Sunny	10	13.90	36.1	23.7	37	5.9	2
Sept-26-N	Sept-26-2015	18:12	6:42	SW-W	Clear			6.2	20.5	59	5.9	2
Sept-27-D	Sept-27-2015	8:21	18:21	N-NE	Sunny	10	12.56	41.9	23.8	42	3.3	2
Sept-27-N	Sept-27-2015	18:38	7:08	N-E	Cloudy			10.2	-	-	3.3	2
Sept-28-D	Sept-28-2015	8:39	18:39	E	Overcast+Rain	0	-	14.1	18.1	82	4.0	2
Sept-28-N	Sept-28-2015	18:47	7:17	E	Overcast+Rain			1.0	17.4	81	4.0	2
Sept-29-D	Sept-29-2015	8:03	18:03	E-SE	Overcast+Rain	0	-	6.7	15.7	88	3.0	2
Sept-29-N	Sept-29-2015	18:33	7:03	SE	Overcast+Rain			0.9	14.7	92	3.0	2
Sept-30-D	Sept-30-2015	8:14	18:14	SW	Cloudy+Rain	3	3.70	19.4	18.1	68	3.2	2
Sept-30-N	Sept-30-2015	18:55	7:25	SW-NW	Cloudy+Rain			13.9	15.5	67	3.2	2
Oct-1-D	Oct-1-2015	7:26	18:31	NW	Sunny	11	17.68	29.2	19.4	27	7.4	3
Oct-1-N	Oct-1-2015	18:41	7:11	NW	Clear			1.7	15.8	51	7.4	3
Oct-2-D	Oct-2-2015	8:50	18:50	NW	Sunny	11	16.00	37.6	24.3	27	4.8	2
Oct-2-N	Oct-2-2015	18:58	7:28	NW	Clear			3.2	18.4	49	4.8	2
Oct-3-D	Oct-3-2015	8:05	18:05	N-S	Sunny	10	14.35	29.1	22.5	35	4.6	2
Oct-3-N	Oct-3-2015	18:30	7:00	SW	Clear			2.1	17.7	66	4.6	2
Oct-4-D	Oct-4-2015	8:20	18:20	SW	Sunny	9	6.40	32.1	21.5	52	2.7	1
Oct-4-N	Oct-4-2015	18:44	7:14	SW	Clear			1.4	17.9	74	2.7	1
Oct-5-D	Oct-5-2015	8:03	18:03	SW	Haze	6	3.89	51.6	21.8	59	3.0	1
Oct-5-N	Oct-5-2015	19:04	7:34	SW	Haze			2.8	18.3	83	3.0	1
Oct-6-D	Oct-6-2015	8:24	18:24	SW-W	Haze	5	3.03	71.4	23.0	60	2.7	1
Oct-6-N	Oct-6-2015	19:25	7:25	SW	Haze			3.4	19.8	81	2.7	1
Oct-7-D	Oct-7-2015	7:55	16:55	SW-NW	Haze	2	1.66	31.6	22.6	68	3.4	2
Oct-7-N	Oct-7-2015	18:00	6:00	NW	Clear			18.9	19.1	24	3.4	2
Oct-8-D	Oct-8-2015	8:07	18:07	NW	Sunny	11	16.11	24.9	17.8	15	7.1	3
Oct-8-N	Oct-8-2015	18:43	6:43	NW	Clear			2.6	14.3	31	7.1	3
Oct-9-D	Oct-9-2015	7:43	17:13	NW	Sunny	11	12.81	18.1	18.7	20	8.3	4
Oct-9-N	Oct-9-2015	17:53	5:23	NW-N	Cloudy			17.9	12.5	30	8.3	4
Oct-10-D	Oct-10-2015	8:10	18:10	NW-N	Sunny	10	12.75	23.8	14.4	24	7.7	4
Oct-10-N	Oct-10-2015	18:38	7:08	N	Cloudy			23.3	15.3	27	7.7	4
Oct-11-D	Oct-11-2015	8:35	18:00	N	Sunny	10	12.63	30.4	20.1	26	7.1	3
Oct-11-N	Oct-11-2015	18:08	6:38	N	Cloudy			5.8	16.6	27	7.1	3
Oct-12-D	Oct-12-2015	7:49	17:31	NW	Sunny	11	14.67	27.4	22.5	20	5.9	1
Oct-12-N	Oct-12-2015	17:40	6:10	NW	Cloudy			2.7	17.8	34	5.9	1
Oct-13-D	Oct-13-2015	8:26	17:48	NW-W	Sunny	11	13.84	22.4	23.7	22	3.7	1
Oct-13-N	Oct-13-2015	17:53	6:23	SW-SE	Cloudy			1.3	17.2	50	3.7	1
Oct-14-D	Oct-14-2015	8:17	17:47	S-E	Cloudy	4	2.99	12.4	20.1	45	3.5	2
Oct-14-N	Oct-14-2015	17:53	6:23	SW-NW	Cloudy			1.1	16.3	64	3.5	2
Oct-15-D	Oct-15-2015	8:28	17:33	W-NW	Sunny	9	8.31	31.9	22.5	38	3.1	2
Oct-15-N	Oct-15-2015	17:39	6:09	W	Cloudy			3.3	19.7	55	3.1	2

SH is the daily solar radiation on a horizontal surface, T is 12-hour averaged temperature, RH is 12-hour averaged relative humidity, MWS is the daily (24-hour) maximum wind speed, and WS is the daily average wind speed.

Table S2. Contents of $PM_{2.5}$, Hg in $PM_{2.5}$ ($PM_{2.5}$-Hg) and Hg isotopic composition of $PM_{2.5}$-Hg.

Name	$PM_{2.5}$ (μg/m^3)	Hg Con. (μg/g)	δ^{202}Hg (‰)	2SD	Δ^{199}Hg (‰)	2SD	Δ^{200}Hg (‰)	2SD	Δ^{201}Hg (‰)	2SD
Sept-15-N	85	0.52	-0.89	0.14	0.05	0.06	0.13	0.04	-0.08	0.07
Sept-16-D	71	0.41	-0.61	0.14	0.30	0.06	0.06	0.04	0.05	0.07
Sept-16-N	88	0.44	-0.53	0.14	-0.05	0.06	0.06	0.04	-0.11	0.07
Sept-17-D	76	0.38	-0.47	0.14	0.21	0.06	0.01	0.04	0.08	0.07
Sept-17-N	94	0.47	-0.27	0.14	-0.08	0.06	0.03	0.04	-0.15	0.07
Sept-18-D	32	0.17	-0.72	0.14	0.90	0.06	0.08	0.04	0.64	0.07
Sept-18-N	43	0.31	-1.29	0.14	0.04	0.06	-0.02	0.04	-0.12	0.09
Sept-19-D	13	0.09								
Sept-19-N	52	0.29	-0.98	0.14	0.09	0.06	0.02	0.04	-0.06	0.07
Sept-20-D	63	0.61	-0.48	0.14	0.16	0.06	0.12	0.04	0.02	0.07
Sept-20-N	63	0.89	-0.59	0.14	0.01	0.06	0.04	0.04	0.06	0.07
Sept-21-D	61	0.48	-0.34	0.14	0.50	0.06	0.05	0.04	0.34	0.07
Sept-21-N	83	0.62	-0.69	0.14	0.10	0.06	0.06	0.04	0.07	0.07
Sept-22-D	95	0.53	-0.40	0.14	0.28	0.06	0.03	0.04	0.18	0.07
Sept-22-N	23	0.31	-0.83	0.14	-0.06	0.06	-0.01	0.04	-0.09	0.07
Sept-23-D	19	0.15								
Sept-23-N	39	0.54	-0.87	0.14	0.17	0.06	0.03	0.04	0.09	0.07
Sept-24-D	84	0.38	-0.25	0.14	0.02	0.06	0.11	0.04	0.03	0.07
Sept-24-N	47	0.20	-0.47	0.14	0.05	0.06	0.06	0.04	-0.11	0.07
Sept-25-D	9	0.38	-0.49	0.14	0.21	0.06	0.18	0.04	0.21	0.07
Sept-25-N	33	0.14	-0.57	0.14	0.42	0.06	0.08	0.04	0.27	0.07
Sept-26-D	24	0.20	-0.37	0.14	1.04	0.06	0.10	0.04	0.71	0.07
Sept-26-N	51	0.44	-0.64	0.18	0.30	0.06	0.09	0.04	0.17	0.07
Sept-27-D	31	0.39	-0.30	0.14	0.76	0.06	0.12	0.04	0.61	0.07
Sept-27-N	46	0.78	-0.62	0.14	0.15	0.06	0.07	0.04	0.08	0.07
Sept-28-D	34	0.32	-0.38	0.14	-0.48	0.06	0.02	0.04	-0.52	0.07
Sept-28-N	34	0.34	-0.32	0.14	-0.46	0.06	0.01	0.04	-0.45	0.07
Sept-29-D	52	0.48	0.29	0.14	0.06	0.06	0.20	0.04	0.26	0.09
Sept-29-N	13	0.36	-0.82	0.14	-0.04	0.06	0.02	0.04	-0.03	0.07
Sept-30-D	14	0.16	-0.23	0.14	-0.13	0.06	0.16	0.04	-0.14	0.07
Sept-30-N	22	0.64	-0.26	0.14	-0.04	0.06	0.08	0.04	-0.05	0.07
Oct-1-D	7	0.12								
Oct-1-N	19	0.67	-0.91	0.14	0.11	0.06	0.11	0.04	0.09	0.07
Oct-2-D	18	0.20	-0.54	0.14	0.29	0.06	0.14	0.04	0.26	0.07
Oct-2-N	31	0.59	-1.49	0.14	0.13	0.06	-0.02	0.04	0.18	0.07
Oct-3-D	19	0.26	-0.21	0.14	0.86	0.06	0.21	0.04	0.59	0.07
Oct-3-N	39	0.59	-0.95	0.14	0.18	0.06	0.07	0.04	0.20	0.07
Oct-4-D	88	0.36	-0.80	0.14	0.27	0.06	0.02	0.04	0.09	0.07
Oct-4-N	119	0.38	-0.97	0.14	-0.11	0.06	0.02	0.04	-0.16	0.07
Oct-5-D	114	0.37	-0.32	0.14	-0.53	0.06	0.09	0.04	-0.64	0.07
Oct-5-N	138	0.53	-0.69	0.14	-0.51	0.06	0.06	0.04	-0.54	0.07
Oct-6-D	156	0.39	-0.09	0.14	-0.40	0.06	0.08	0.04	-0.57	0.07
Oct-6-N	158	0.44	0.16	0.14	-0.15	0.06	0.10	0.04	-0.12	0.07
Oct-7-D	138	0.47	0.20	0.14	0.69	0.06	0.08	0.04	0.42	0.07
Oct-7-N	128	0.46	0.52	0.14	0.55	0.06	0.14	0.04	0.39	0.07
Oct-8-D	4	0.30	-0.22	0.14	0.32	0.06	0.19	0.04	0.20	0.07
Oct-8-N	16	0.24	0.55	0.14	-0.07	0.06	0.09	0.04	0.01	0.07
Oct-9-D	24	0.43	-0.47	0.14	0.04	0.06	0.07	0.04	0.12	0.07
Oct-9-N	17	0.08								
Oct-10-D	14	0.19	-0.82	0.14	0.33	0.06	0.08	0.04	0.55	0.07
Oct-10-N	8	0.26	-0.61	0.14	0.32	0.06	0.11	0.04	0.28	0.07
Oct-11-D	12	0.10								
Oct-11-N	15	0.38	-0.42	0.14	0.17	0.06	0.14	0.04	0.20	0.07
Oct-12-D	10	0.27	-0.79	0.14	0.28	0.06	0.12	0.04	0.27	0.07
Oct-12-N	26	1.22	-0.90	0.14	-0.03	0.06	0.05	0.04	-0.03	0.07
Oct-13-D	19	0.43	-0.70	0.14	0.23	0.06	0.01	0.04	0.16	0.07
Oct-13-N	60	0.89	-0.80	0.14	-0.01	0.06	0.06	0.04	-0.06	0.07
Oct-14-D	50	0.37	-0.78	0.14	0.01	0.06	-0.01	0.04	0.00	0.07
Oct-14-N	82	0.49	-1.21	0.14	-0.20	0.06	-0.02	0.04	-0.18	0.07
Oct-15-D	50	0.34	-0.60	0.14	0.57	0.06	0.08	0.04	0.52	0.07
Oct-15-N	95	0.33	-0.37	0.14	0.21	0.06	0.07	0.04	0.33	0.07

Table S3. The below results of Paired Samples T-Test and Independent Samples T-Test were obtained using the IBM SPSS Statistics Version 22. The paired samples were consecutive day and night $PM_{2.5}$ samples, for example, Sept-16-D and Sept-16-N were paired samples.

Paired Samples Test

Day - Night	Paired Differences					t	df	Sig. (2-tailed)
	Mean	Std. Deviation	Std. Error Mean	95% Confidence Interval of the Difference				
				Lower	Upper			
$PM_{2.5}$	-2.06667	78.67959	14.36486	-31.44611	27.31278	-0.144	29	0.887
Hg Con.	-0.15263	0.27183	0.04963	-0.25414	-0.05113	-3.075	29	0.005
$\delta^{202}Hg$	0.16960	0.41413	0.08283	-0.00134	0.34054	2.048	24	0.052
$\Delta^{199}Hg$	0.24400	0.28384	0.05677	0.12684	0.36116	4.298	24	0.000
$\Delta^{200}Hg$	0.04120	0.06412	0.01282	0.01473	0.06767	3.213	24	0.004

Independent Samples Test

Day vs Night	Mean Difference	Std. Error Difference	95% Confidence Interval of the Difference		t	df	Sig. (2-tailed)
			Lower	Upper			
$PM_{2.5}$	-2.57742	22.46315	-47.52607	42.37123	-0.115	59	0.909
Hg Con.	-0.15408	0.04966	-0.25393	-0.05423	-3.103	47.858	0.003
$\delta^{202}Hg$	0.20549	0.10385	-0.00272	0.41370	1.979	54	0.053
$\Delta^{199}Hg$	0.21982	0.08777	0.04209	0.39755	2.505	37.666	0.017
$\Delta^{200}Hg$	0.03464	0.01437	0.00582	0.06346	2.410	54	0.019

Table S4. Calculated GOM concentrations of day and night samples. The value of GOM concentrations higher at night than the consecutively days are in bold text.

Daytime samples	Ave. T (ºC)	Hg Con. ($\mu g\ g^{-1}$)	*K* $m^3\ \mu g^{-1}$	GOM $pg\ m^{-3}$	Nighttime samples	Ave. T (ºC)	Hg Con. ($\mu g\ g^{-1}$)	*K* $m^3\ \mu g^{-1}$	GOM $pg\ m^{-3}$
					Sept-15-N	19.8	0.52	0.035	15
Sept-16-D	24.1	0.41	0.026	16	Sept-16-N	21.1	0.44	0.032	14
Sept-17-D	24.8	0.38	0.025	15	Sept-17-N	22.6	0.47	0.029	**16**
Sept-18-D	27.3	0.17	0.021	8.0	Sept-18-N	21.7	0.31	0.030	**10**
Sept-19-D	26.1	0.09	0.023	3.9	Sept-19-N	21.7	0.29	0.030	10
Sept-20-D	24.5	0.61	0.025	24	Sept-20-N	21.9	0.89	0.030	**30**
Sept-21-D	25.2	0.48	0.024	20	Sept-21-N	22.6	0.62	0.029	**22**
Sept-22-D	22.9	0.53	0.028	19	Sept-22-N	18.3	0.31	0.038	8.1
Sept-23-D	23.9	0.15	0.026	5.7	Sept-23-N	21.6	0.54	0.031	**18**
Sept-24-D	23	0.38	0.028	14	Sept-24-N	17.7	0.2	0.040	5.0
Sept-25-D	24.4	0.38	0.025	15	Sept-25-N	17.3	0.14	0.041	3.4
Sept-26-D	23.7	0.2	0.027	7.5	Sept-26-N	20.5	0.44	0.033	13
Sept-27-D	23.8	0.39	0.026	15	Sept-27-N	-	0.78		
Sept-28-D	18.1	0.32	0.039	8	Sept-28-N	17.4	0.34	0.041	8.4
Sept-29-D	15.7	0.48	0.046	11	Sept-29-N	14.7	0.36	0.049	7.4
Sept-30-D	18.1	0.16	0.039	4.1	Sept-30-N	15.5	0.64	0.046	**14**
Oct-1-D	19.4	0.12	0.035	3.4	Oct-1-N	15.8	0.67	0.045	**15**
Oct-2-D	24.3	0.2	0.026	7.8	Oct-2-N	18.4	0.59	0.038	**16**
Oct-3-D	22.5	0.26	0.029	9.0	Oct-3-N	17.7	0.59	0.040	**15**
Oct-4-D	21.5	0.36	0.031	12	Oct-4-N	17.9	0.38	0.039	10
Oct-5-D	21.8	0.37	0.030	12	Oct-5-N	18.3	0.53	0.038	**14**
Oct-6-D	23	0.39	0.028	14	Oct-6-N	19.8	0.44	0.035	13
Oct-7-D	22.6	0.47	0.029	16	Oct-7-N	19.1	0.46	0.036	13
Oct-8-D	17.8	0.3	0.040	7.6	Oct-8-N	14.3	0.24	0.050	4.8
Oct-9-D	18.7	0.43	0.037	12	Oct-9-N	12.5	0.08	0.057	1.4
Oct-10-D	14.4	0.19	0.050	3.8	Oct-10-N	15.3	0.26	0.047	**5.5**
Oct-11-D	20.1	0.1	0.034	3.0	Oct-11-N	16.6	0.38	0.043	8.9
Oct-12-D	22.5	0.27	0.029	9.4	Oct-12-N	17.8	1.22	0.040	**31**
Oct-13-D	23.7	0.43	0.027	16	Oct-13-N	17.2	0.89	0.041	**22**
Oct-14-D	20.1	0.37	0.034	11	Oct-14-N	16.3	0.49	0.044	11
Oct-15-D	22.5	0.34	0.029	12	Oct-15-N	19.7	0.33	0.035	9.5

Figure S1. NOAA-HYSPLIT model shown back trajectories for 30 day-night $PM_{2.5}$ sample pairs collected during Sep. 16th to Oct. 15th 2015 from urban center of Beijing, China. Arriving air masses of 500 m above ground level (AGL) were calculated on website of http://ready.arl.noaa.gov/hypub-bin/trajtype.pl?runtype=archive.

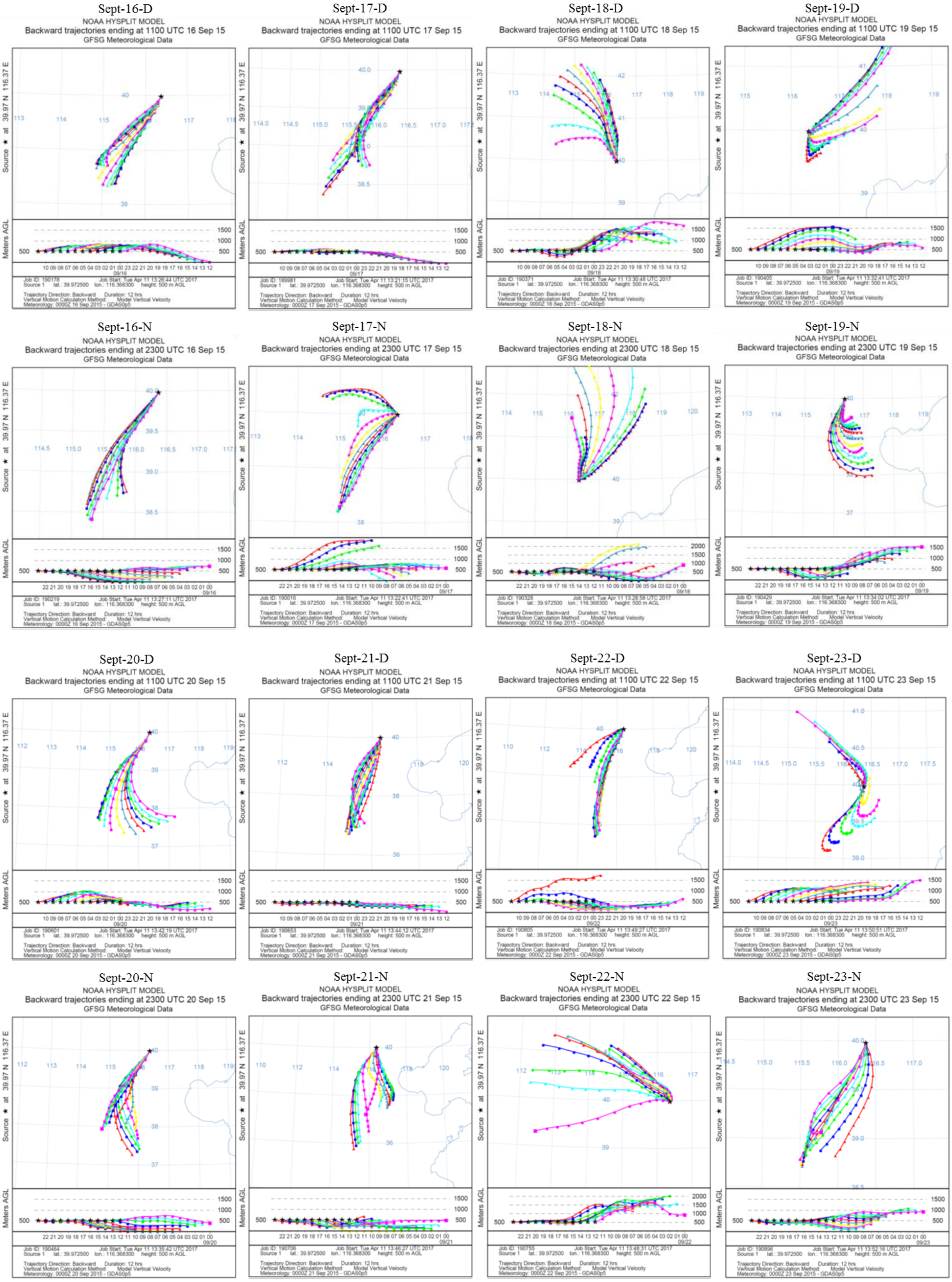

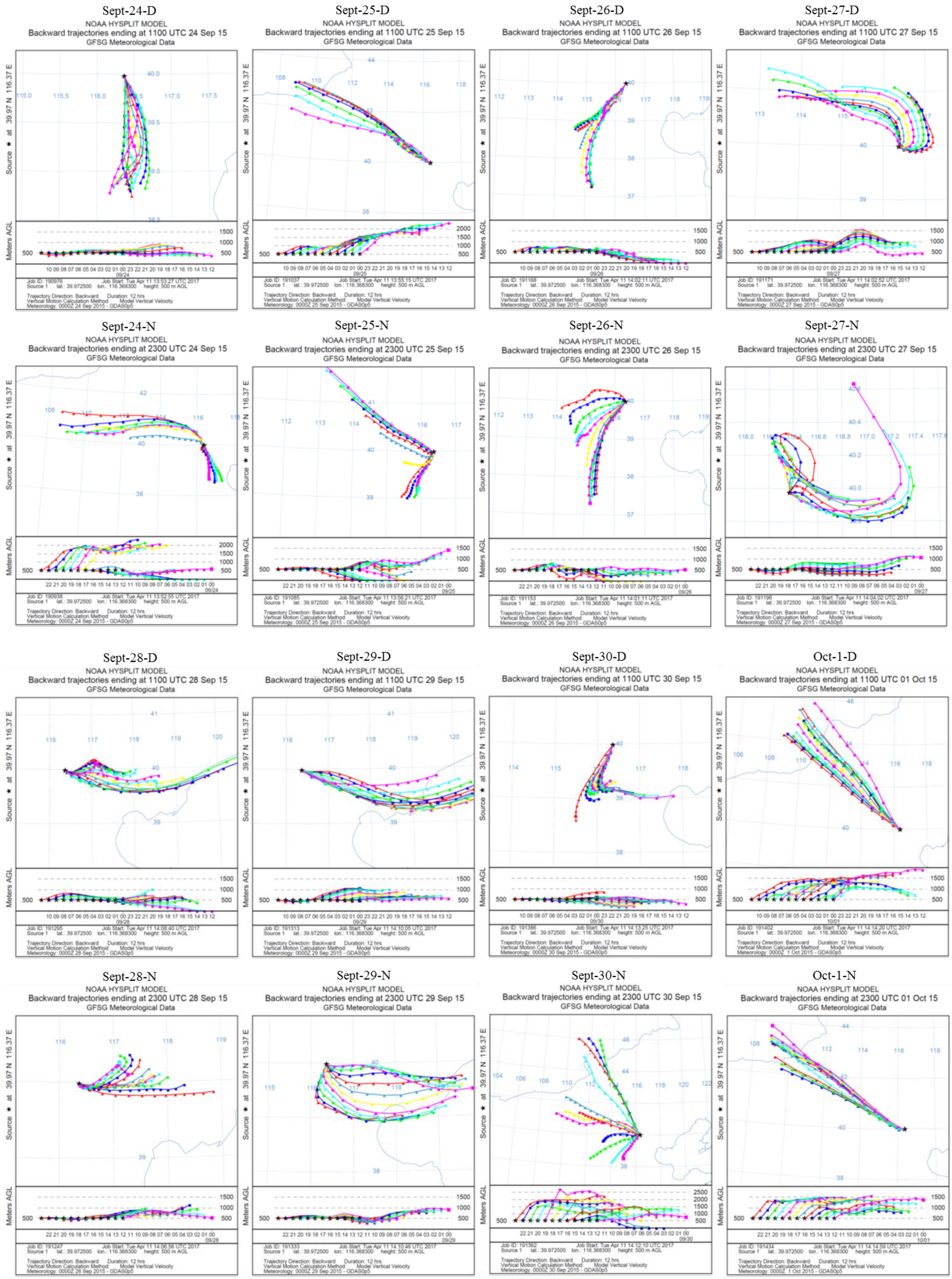
Sept-24-D
NOAA HYSPLIT MODEL
Backward trajectories ending at 1100 UTC 24 Sep 15
GFSG Meteorological Data
Sept-25-D
NOAA HYSPLIT MODEL
Backward trajectories ending at 1100 UTC 25 Sep 15
GFSG Meteorological Data
Sept-26-D
NOAA HYSPLIT MODEL
Backward trajectories ending at 1100 UTC 26 Sep 15
GFSG Meteorological Data
Sept-27-D
NOAA HYSPLIT MODEL
Backward trajectories ending at 1100 UTC 27 Sep 15
GFSG Meteorological Data
Sept-24-N
NOAA HYSPLIT MODEL
Backward trajectories ending at 2300 UTC 24 Sep 15
GFSG Meteorological Data
Sept-25-N
NOAA HYSPLIT MODEL
Backward trajectories ending at 2300 UTC 25 Sep 15
GFSG Meteorological Data
Sept-26-N
NOAA HYSPLIT MODEL
Backward trajectories ending at 2300 UTC 26 Sep 15
GFSG Meteorological Data
Sept-27-N
NOAA HYSPLIT MODEL
Backward trajectories ending at 2300 UTC 27 Sep 15
GFSG Meteorological Data
Sept-28-D
NOAA HYSPLIT MODEL
Backward trajectories ending at 1100 UTC 28 Sep 15
GFSG Meteorological Data
Sept-29-D
NOAA HYSPLIT MODEL
Backward trajectories ending at 1100 UTC 29 Sep 15
GFSG Meteorological Data
Sept-30-D
NOAA HYSPLIT MODEL
Backward trajectories ending at 1100 UTC 30 Sep 15
GFSG Meteorological Data
Oct-1-D
NOAA HYSPLIT MODEL
Backward trajectories ending at 1100 UTC 01 Oct 15
GFSG Meteorological Data
Sept-28-N
NOAA HYSPLIT MODEL
Backward trajectories ending at 2300 UTC 28 Sep 15
GFSG Meteorological Data
Sept-29-N
NOAA HYSPLIT MODEL
Backward trajectories ending at 2300 UTC 29 Sep 15
GFSG Meteorological Data
Sept-30-N
NOAA HYSPLIT MODEL
Backward trajectories ending at 2300 UTC 30 Sep 15
GFSG Meteorological Data
Oct-1-N
NOAA HYSPLIT MODEL
Backward trajectories ending at 2300 UTC 01 Oct 15
GFSG Meteorological Data

Oct-2-D

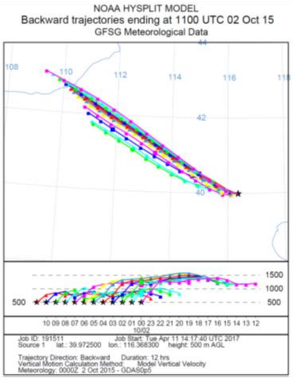

Oct-3-D

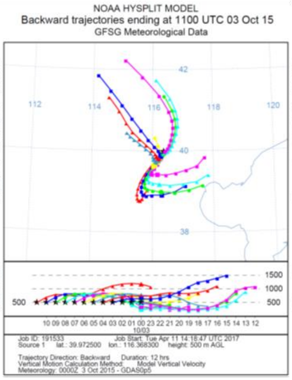

Oct-4-D

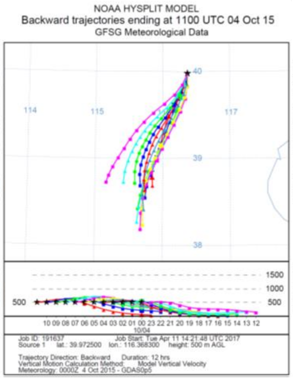

Oct-5-D

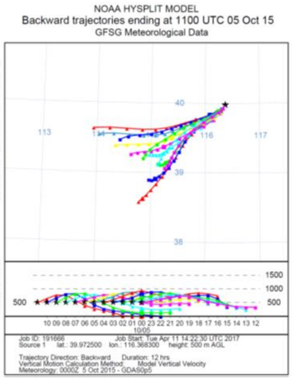

Oct-2-N

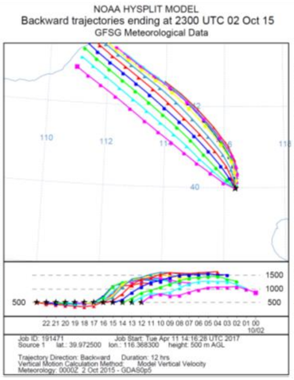

Oct-3-N

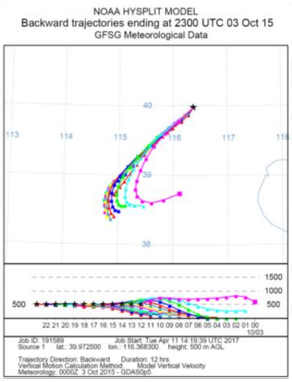

Oct-4-N

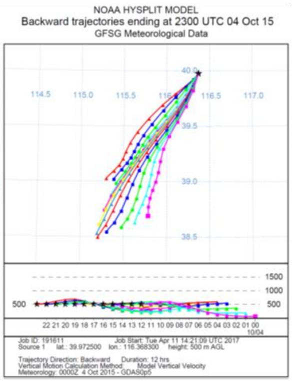

Oct-5-N

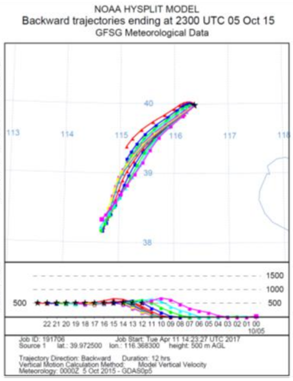

Oct-6-D

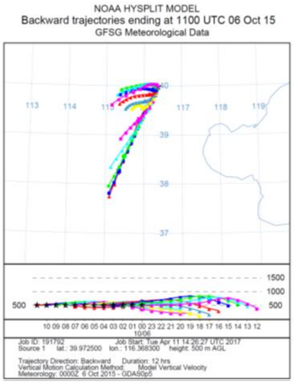

Oct-7-D

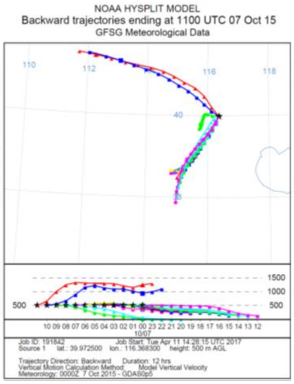

Oct-8-D

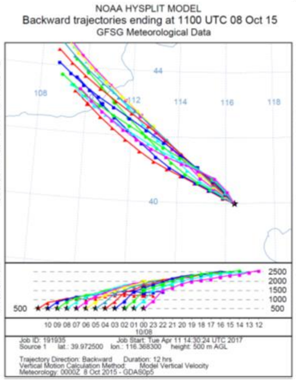

Oct-9-D

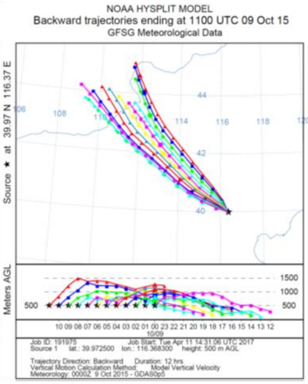

Oct-6-N

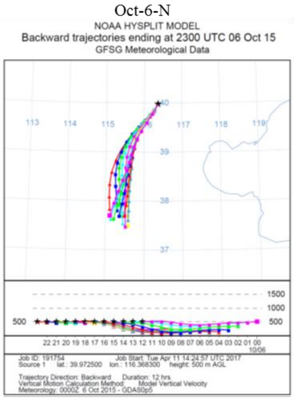

Oct-7-N

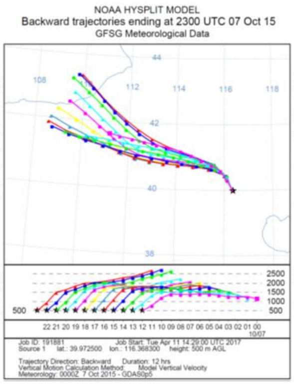

Oct-8-N

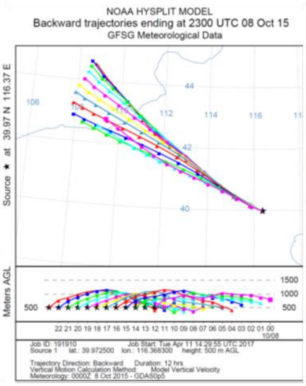

Oct-9-N

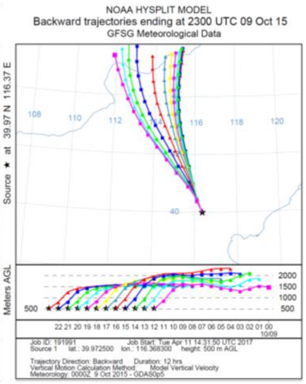

Oct-10-D

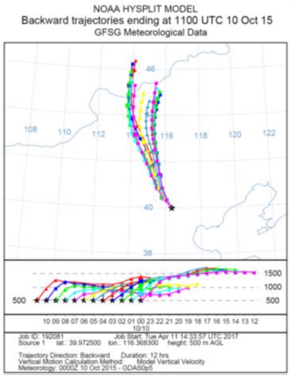

Oct-11-D

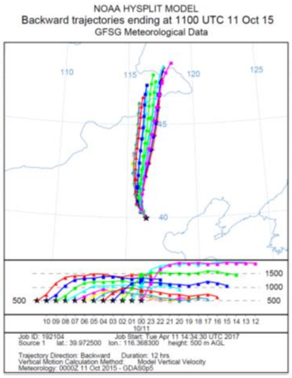

Oct-12-D

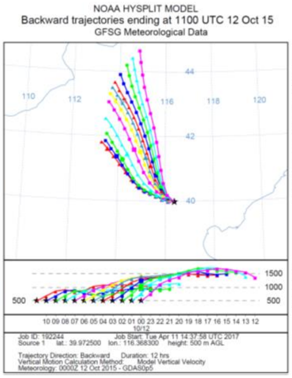

Oct-13-D

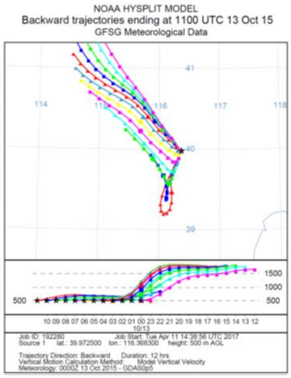

Oct-10-N

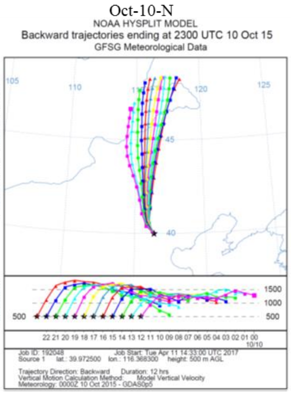

Oct-11-N

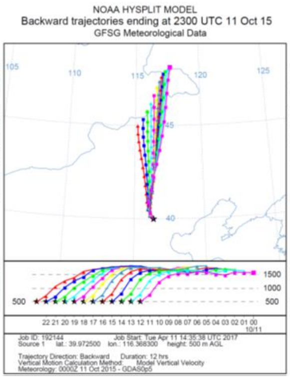

Oct-12-N

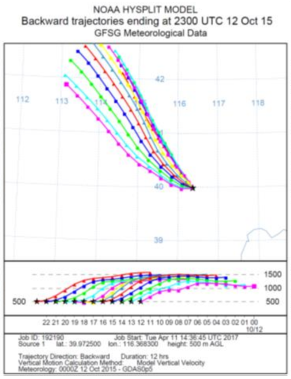

Oct-13-N

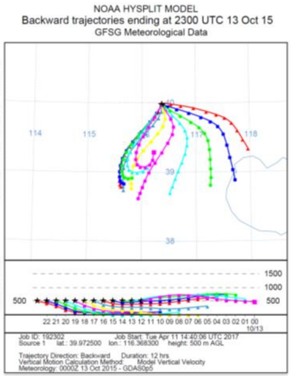

Oct-14-D

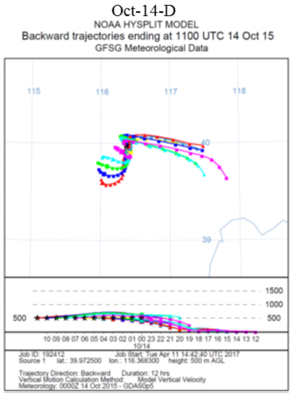

Oct-15-D

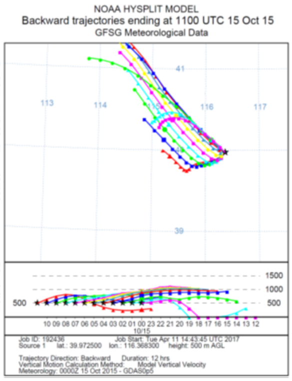

Oct-14-N

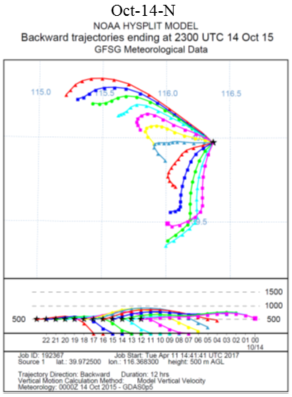

Oct-15-N

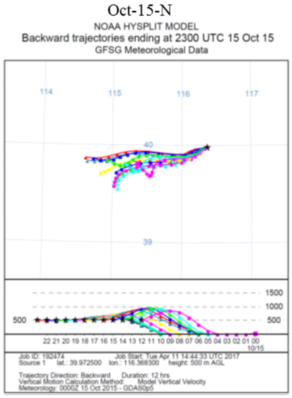

Figure S2. $\Delta^{199}Hg$ (‰) versus the content of Hg in $PM_{2.5}$ ($\mu g\ g^{-1}$) for different subsets of $PM_{2.5}$ samples: a) all data, b) North-West (N-W), c) South-East (S-E) and d) All sunny days (Sun), with Spearman Correlation Coefficient (*R*) and 1-tailed significant (*p*). The red circles are for daytime samples, while blue circles are for night samples.

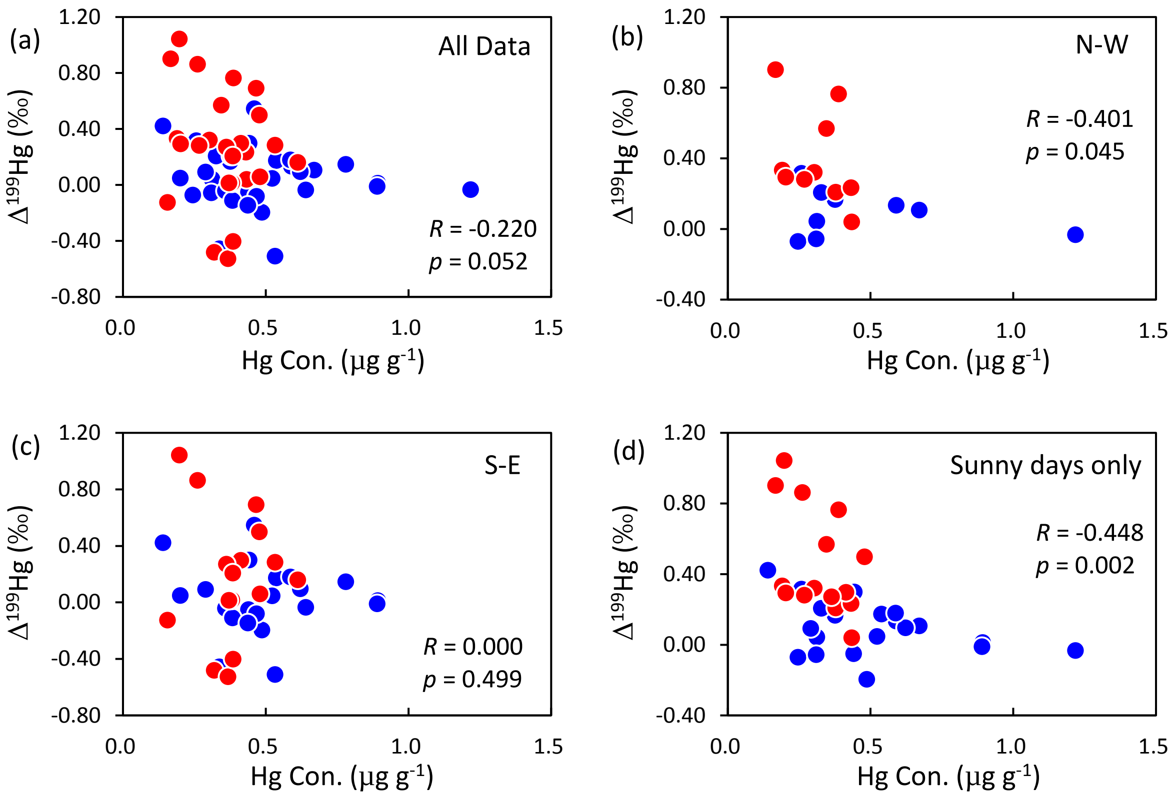

Figure S3. $\Delta^{199}Hg$ (‰) versus $\delta^{202}Hg$ (‰) for different subsets of $PM_{2.5}$ samples: a) all data, b) North-West (N-W), c) South-East (S-E) and d) All sunny days (Sun), with Spearman Correlation Coefficient (R) and 1-tailed significant (p). The red circles are for daytime samples, while the blue circles are for night samples.

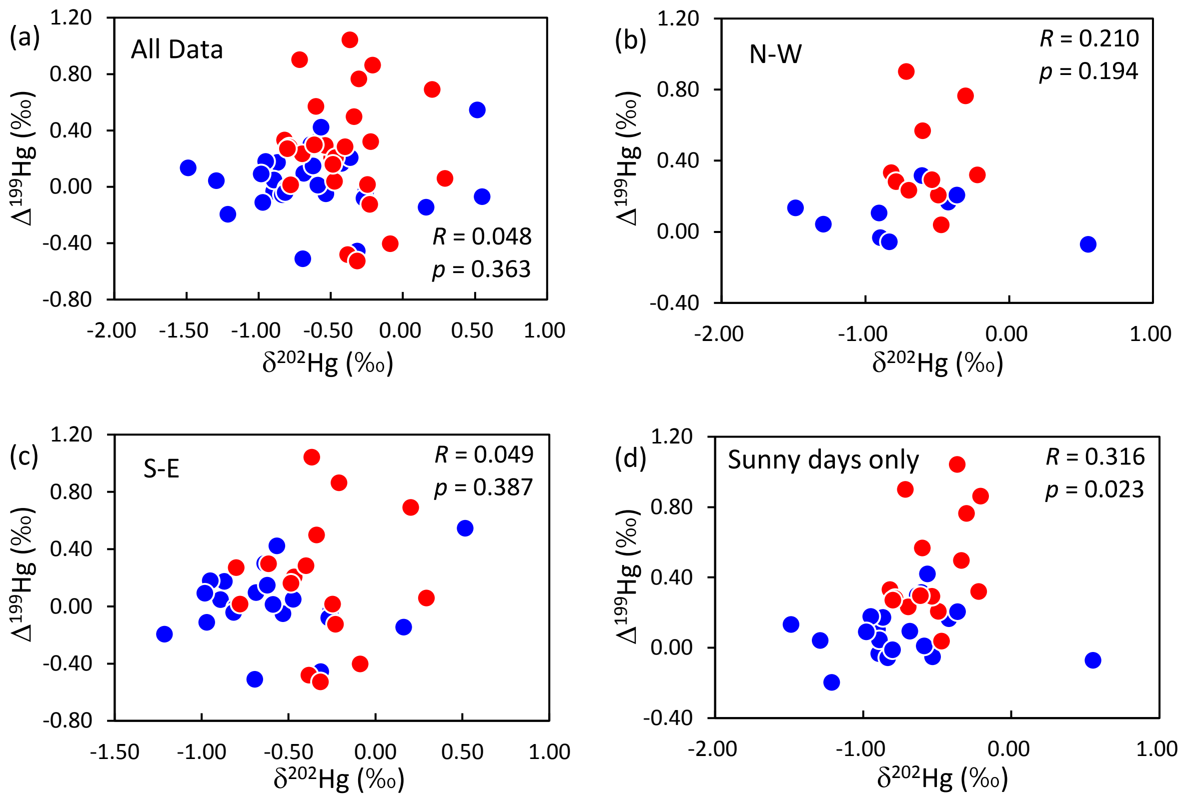

Figure S4. $\Delta^{199}Hg$ values of daytime $PM_{2.5}$ samples versus sunshine duration (hr).

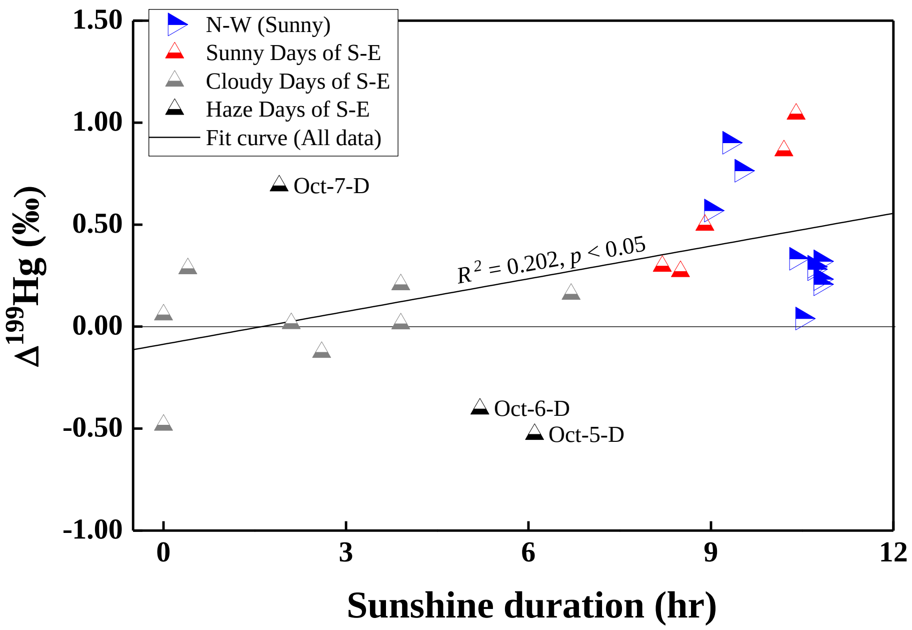

180 **Figure S5.** $\Delta^{199}Hg$ values of daytime $PM_{2.5}$ samples versus atmospheric ozone content (ppbv).

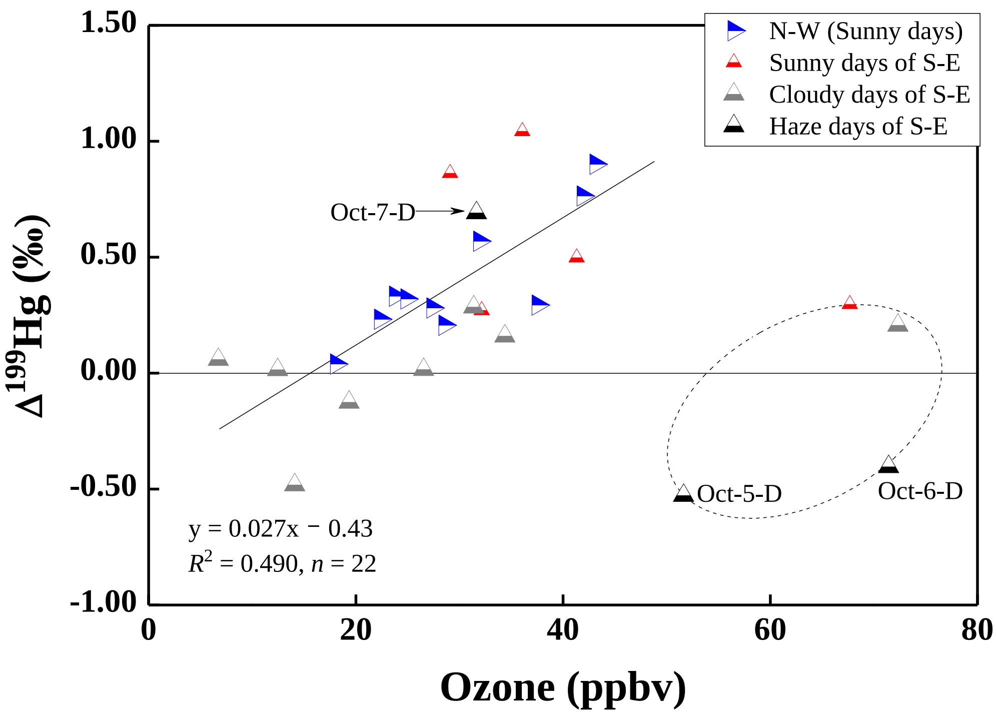

Figure S6. $\Delta^{199}Hg$ (‰) versus $\Delta^{200}Hg$ (‰) for different subsets of $PM_{2.5}$ samples: a) all data, b) North-West (N-W), c) South-East (S-E) and d) All sunny days (Sun). The red circles are for daytime samples, while the blue circles are for night samples. Positive correlations between $\Delta^{199}Hg$ and $\Delta^{200}Hg$ can be seem in each subsets, with Spearman Correlation Coefficient (R) and 1-tailed significant (p).

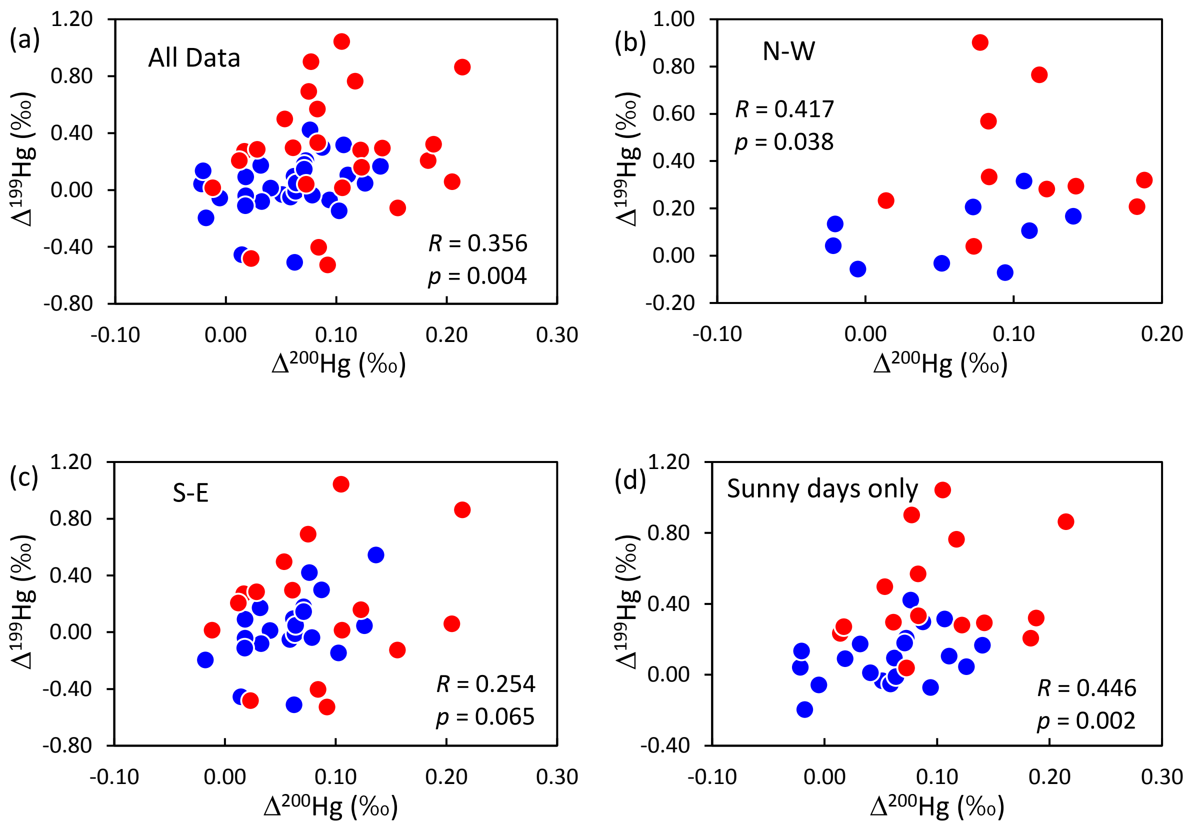

Figure S7. Δ^{200}Hg (‰) versus δ^{202}Hg (‰) for different subsets of $PM_{2.5}$ samples: a) all data, b) North-West (N-W), c) South-East (S-E) and d) All sunny days (Sun). The red circles are for daytime samples, while the blue circles are for night samples. Positive correlations between Δ^{200}Hg and δ^{202}Hg can be seem in each subsets with Spearman Correlation Coefficient (*R*) and 1-tailed significant (*p*).

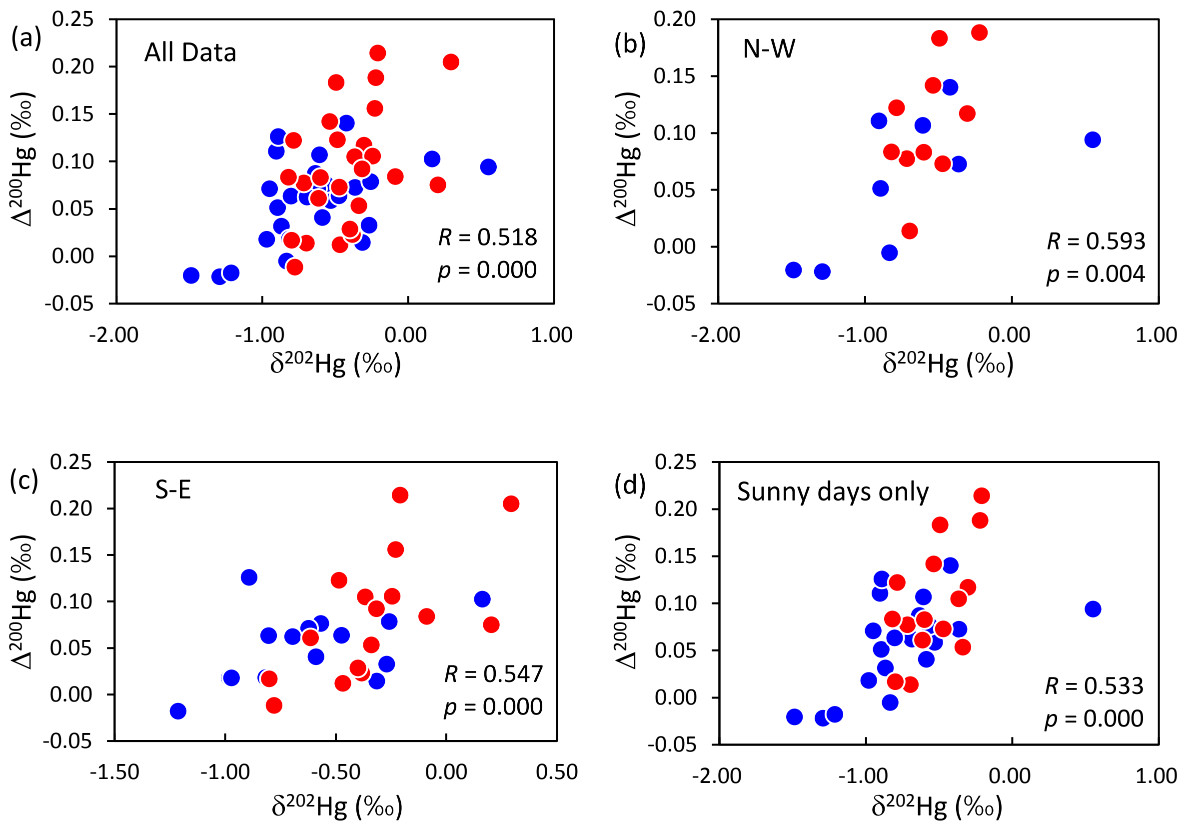

REFERENCES

Amos, H. M., Jacob, D. J., Holmes, C. D., Fisher, J. A., Wang, Q., Yantosca, R. M., Corbitt, E. S., Galarneau, E., Rutter, A. P., Gustin, M. S., Steffen, A., Schauer, J. J., Graydon, J. A., St Louis, V. L., Talbot, R. W., Edgerton, E. S., Zhang, Y., and Sunderland, E. M.: Gas-particle partitioning of atmospheric Hg(II) and its effect on global mercury deposition, Atmos. Chem. Phys., 12, 591-603, 2012.

Blum, J. D., and Bergquist, B. A.: Reporting of variations in the natural isotopic composition of mercury, Anal. Bioanal. Chem., 388, 353-359, 2007.

Huang, Q., Liu, Y. L., Chen, J. B., Feng, X. B., Huang, W. L., Yuan, S. L., Cai, H. M., and Fu, X. W.: An improved dual-stage protocol to pre-concentrate mercury from airborne particles for precise isotopic measurement, J. Anal. At. Spectrom., 30, 957-966, 2015.

Huang, Q., Chen, J., Huang, W., Fu, P., Guinot, B., Feng, X., Shang, L., Wang, Z., Wang, Z., Yuan, S., Cai, H., Wei, L., and Yu, B.: Isotopic composition for source identification of mercury in atmospheric fine particles, Atmos. Chem. Phys., 16, 11773-11786, 2016.

Xiang, Y., Zhang, T., Liu, J., Lv, L., Dong, Y., and Chen, Z.: Atmosphere boundary layer height and its effect on air pollutants in Beijing during winter heavy pollution, Atmos. Res., 215, 305-316, https://doi.org/10.1016/j.atmosres.2018.09.014, 2019.